Technology and Health Care 17 (2009) 421–444
DOI 10.3233/THC-2009-0563
IOS Press

Bioimaging

Chapter 1: Diagnostic Medical Imaging: X-ray projection technique, image subtraction method, direct digital x-ray imaging, computed tomography (CT)

Peter F. Niederer
Institute of Biomedical Engineering, University and ETH Zurich, Gloria strasse 35, CH-8092 Zurich, Swtzerland
E-mail: peter.niederer@biomed.ee.ethz.ch

1. Introduction

In 1896 W.C. Röntgen announced the discovery of the potential of an at that time yet unknown type of radiation to penetrate materials and to cause opacification of photographic plates (after development). It turned out that various biological tissues attenuated this radiation differently such that the generation of projections of the human body onto a photographic plate was possible (Fig. 1.1). As the physical nature of the radiation was unknown, it was said to consist of "x-rays" – a designation which is still in use today.

A further milestone was the introduction of computed x-ray tomography by G.N. Hounsfield in 1973 which for the first time allowed to produce cross sections of the human body for diagnostic purposes *in vivo* and noninvasively apart from the application of a radiation dose (Fig. 1.2).

The x-rays used for diagnostic purposes in medicine are electromagnetic waves with a photon energy between 30–200 KeV typically. "X-ray" was until a few years ago the most often applied medical imaging technology. Since then, methods on the basis of ultrasound (in contrast to x-ray non-ionizing) have become more often used. In addition, MRI (Magnetic Resonance Imaging) is of rapidly increasing significance in medical imaging, in particular as with the combination MRI/MRS (MR Imaging and Spectroscopy) also functional examinations can be made. The combination of x-ray CT (Computed Tomography) with PET (Positron Emission Tomography), in turn, has in recent years fostered significant and novel clinical applications for functional investigations.

The radiation dose which is delivered to the patient is always of concern; it should be as small as possible. An enormous progress has been achieved through the years such that today a "simple" x-ray image can be produced with the aid of a radiation dose which can be considered harmless (Fig. 1.3).

0928-7329/09/$17.00 © 2009 – IOS Press and the authors. All rights reserved

Figure 1.1: X-ray of the hand of W.C. Róntgen's wife.

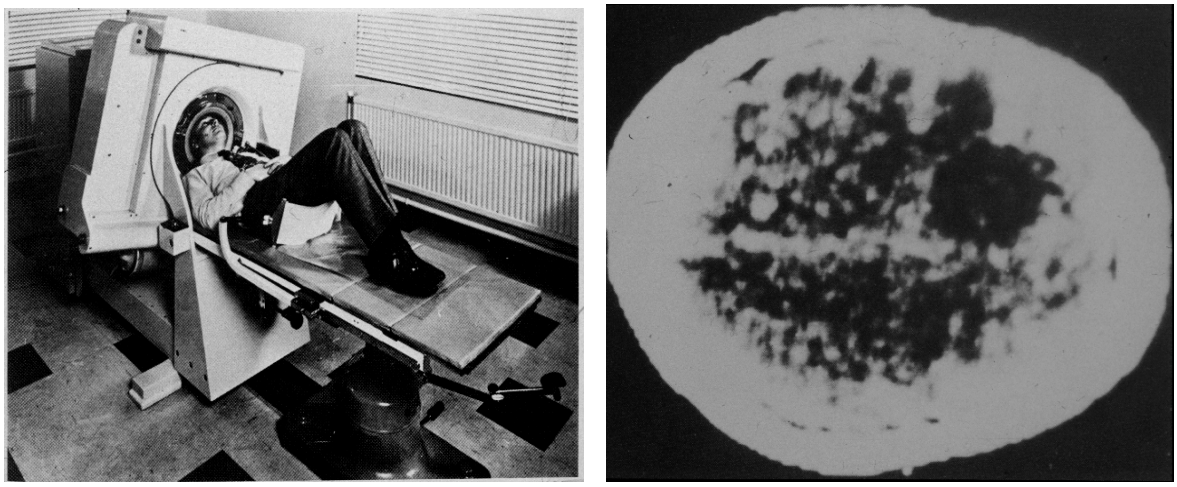

Figure 1.2: First CT scanner (1973).

2. Generation of x-rays

X-rays for diagnostic purposes in clinical medicine are usually generated with the aid of a x-ray tube (in order to produce the much higher-energy therapeutic radiation in the MeV-range, linear accelerators are mostly used). In such a tube whose interior is highly evacuated (the pressure is typically 10^{-6} Torr $\sim 10^{-4}$ Pa), electrons are "evaporated" from a wolfram cathode by heating (the melting temperature of wolfram is 3400°C) and exposed to an anode voltage, V, of some 30'000 to 200'000 Volt for acceleration towards the anode. The electrons thereby obtain a kinetic energy of 30 to 200 keV (electron charge,

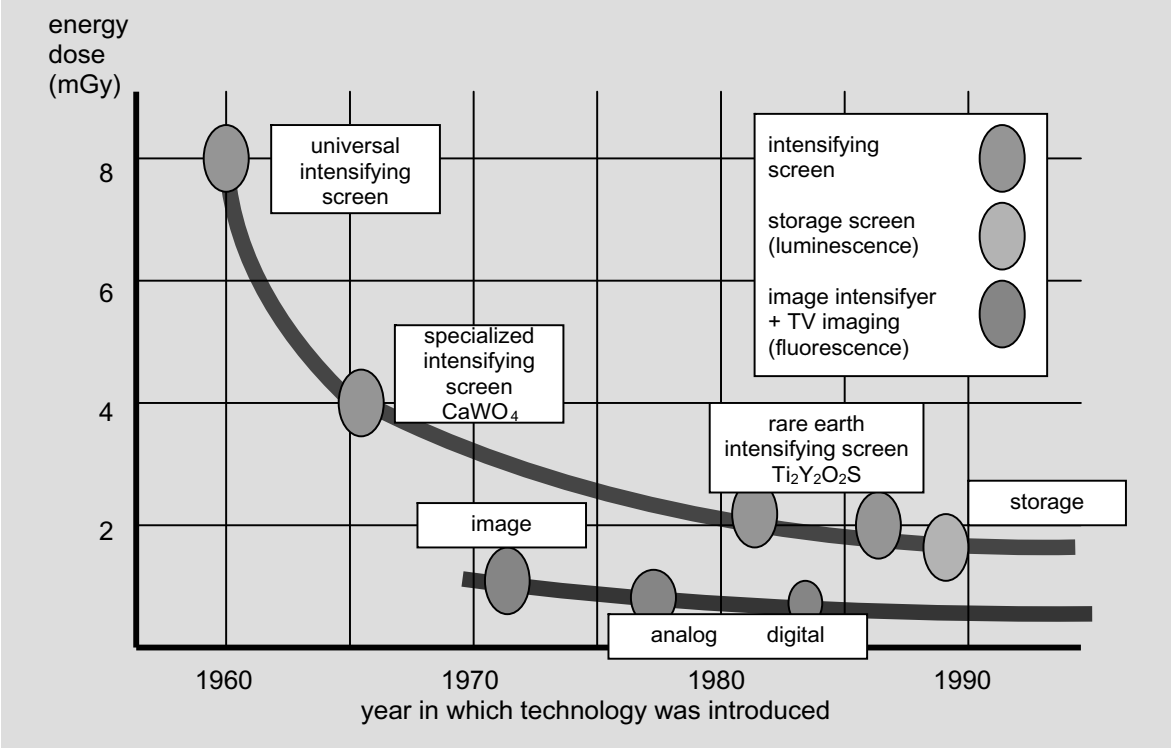

Figure 1.3: Typical radiation dose delivered for a x-ray projection image.

e, times potential difference, V). The geometric arrangement of the cathode along with the spatial characteristics of the accelerating field are designed such that the electron beam hits the target (anode) in a carefully outlined distribution (focal spot, see later).

When the accelerated electrons are being absorbed by the target material, x-ray is generated due to two effects, *viz.*,

– bremsstrahlung
– characteristic radiation

Besides that, most of the kinetic energy of the electrons is converted into heat (see below).

Bremsstrahlung is emitted, when fast electrons interact with the strong (positive) electric field of atomic nuclei. The electrons are deflected in this field and radiate electromagnetic waves in the form of photons. The electrons thereby loose kinetic energy, i.e., are braked down (therefore the German expression “bremsstrahlung”). The spectrum of this radiation is continuous because the effect depends essentially on the distance at which the electron passes the nucleus and each distance has the same probability. The spectrum therefore extends from (theoretically) zero up to the maximal possible photon energy, E_{max}, which occurs when the electron looses its entire kinetic energy in one step.

The spectrum associated with a thin target is constant, because most electrons, while traversing the thin layer, are involved in only one scattering process, thereby loosing part of their energy such that each portion of energy from zero to the maximum has the same probability. In a thick target, in turn, the spectrum is linearly decreasing with $E \rightarrow E_{max}$, because except for a few electrons which are backscattered at the surface layer all electrons always loose their entire kinetic energy in various single steps of different intensity (there are more small steps possible than large ones). According to

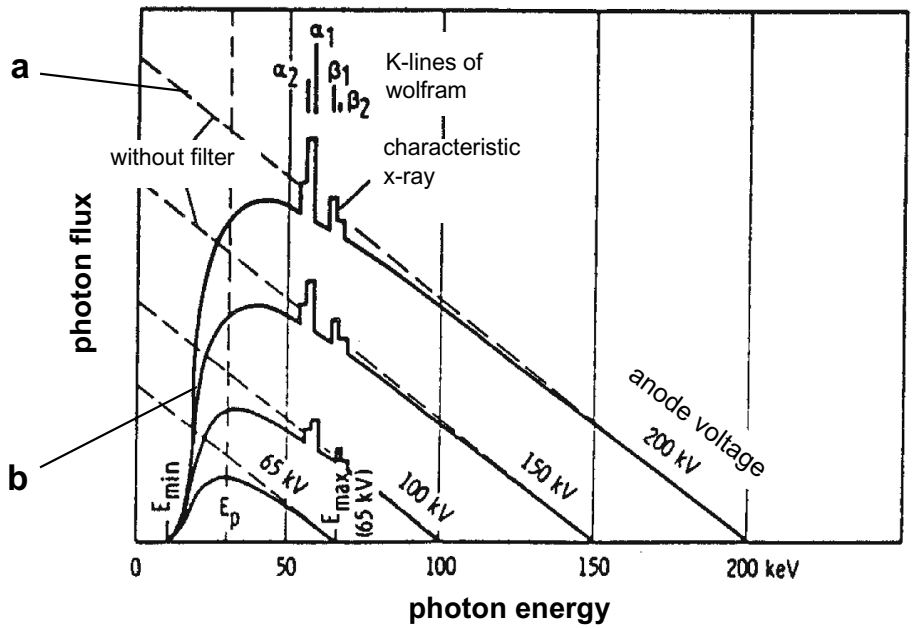

Figure 2.1: Typical spectrum of an x-ray tube (photon flux as function of energy) a: Bremsstrahlung (theoretical, without prefilter) b: Spectrum at different anode voltages; wolfram target, 1 mm Al prefilter (bremsstrahlung + superimposed characteristic x-ray).

$E_{\max} = e\,V = h\,\nu_{\max}$ (h: Planck's constant,
ν: photon frequency
e: electron charge)

the minimal wavelength, λ_{min}, which is associated with the maximal photon energy E_{max}, is (speed of light $c = \lambda\nu$)

$$\lambda_{min} = hc/eV$$

With $h = 6.63{\cdot}10^{-34}$ W sec^2
$c = 3{\cdot}10^{8}$ m/sec
$V = 100$ kV
$e = 1.6{\cdot}10^{-19}$ Clb

one obtains $\lambda_{\min} = 12.4{\cdot}10^{-2}$ Å $= 1.24$ nm. Typical spectra are shown in Fig. 2.1. The decrease at low energies is on the one hand due to self-absorption in the target material, and on the other to prefiltering (low energy photons are removed purposely because they do not contribute to image formation but just increase the radiation dose imparted to the patient, see below and 3.2. Absorption of x-rays).

The electrons hitting and penetrating the target not only interact with the nuclei of the target material, but also with the electrons thereof. Electrons may thereby be ejected from their orbit, and radiation quanta are emitted during subsequent recombination. Since the orbits have defined energy levels, the quanta have energies corresponding to the various orbits (K, L,. . . , Fig. 2.1) and the spectrum consists accordingly of lines (characteristic x-ray).

Most of the kinetic energy is however converted into heat ($\sim$99%) in the target material (electromagnetic waves with long wavelengths, largely due to interactions with free and weakly bound electrons of the target material). As mentioned above, the low-energy part of the spectrum is usually removed with the aid of prefilters (Al or Cu sheet metal plates) in order to reduce the radiation dose.

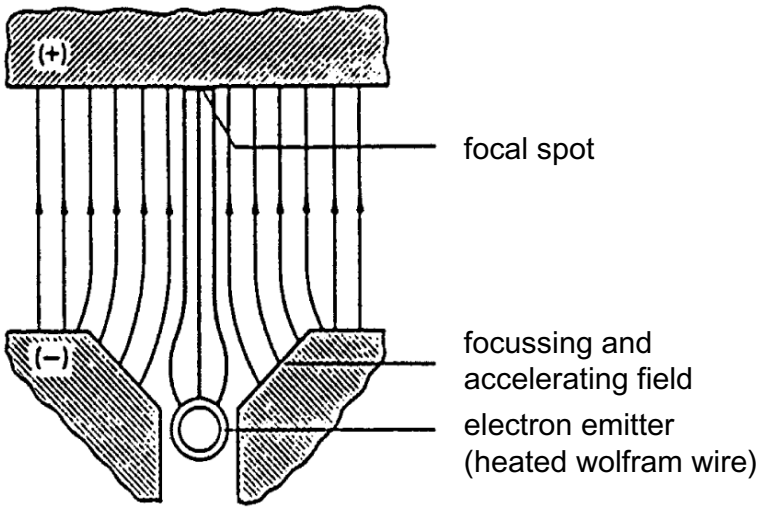

Figure 2.2: Focussing of electrons, originating from the cathode ($-$) onto the focal spot of the anode ($+$).

The radiation beam is strictly speaking not continuous as it is composed of a large number of incoherent electromagnetic wave packets (photons; the scattering processes in the target material occur independently from one another). The number of photons is so large, however, that quantum noise is not of importance (exception: image subtraction, see later).

There is a great variety of x-ray tubes available for different medical applications; yet, the basic physical effects are always the same. Material problems are prominent (hot cathode, extreme local heating of the anode). At a typical anode current (= electron current) of $I = 100$ mA and a voltage $U =$ 100 kV the power deposited in the anode is

$$E = I \cdot U = 10kW$$

A projection image with a good resolution is only obtained if the focal spot (Fig. 2.2) is small (another possibility is to locate the x-ray tube as far away from the object as possible; this is however limited due to practical reasons). X-rays propagate along straight paths, there exist no x-ray "lenses" for practical medical imaging purposes. The electrons are focused on the focal spot by the suitably shaped accelerating field. Since all the heat is produced in the focal spot, a small spot is difficult to achieve. Therefore, the anode is usually inclined with respect to the electron beam such that the focal spot can be extended (Fig. 2.3) and the heat production is distributed accordingly. In the direction of the projection, the focal area still has a localised aspect (for special purposes, also tubes with a line focus are used). In addition, in high power tubes the anode rotates (5000 min^{-1} typ.) such that the focal spot is not static (Fig. 2.3).

The heat is disposed of by diffusion through the anode as well as by radiation. The latter obeys the Stefan-Boltzmann law according to which a black body radiates the energy per unit area, W, as

$W = \sigma T^4$ (σ = Stefan-Boltzmann constant, $5.7 \cdot 10^{-12}$ W/cm^{2}K^4,

T = temperature)

At $T = 2500°$ K and an emission efficiency of 0.7 (graphite; the emission efficiency of a black body is 1) the radiated power per unit area is $W \sim 200$ W/cm^2. Even under normal operating conditions, the anode may be extremely loaded thermally (Fig. 2.4).

The further away the tube is positioned from the object, the sharper the images become since the focal spot has always a certain size. In contrast, the recording medium, e.g., a x-ray film cassette should be located as closely as possible behind the object.

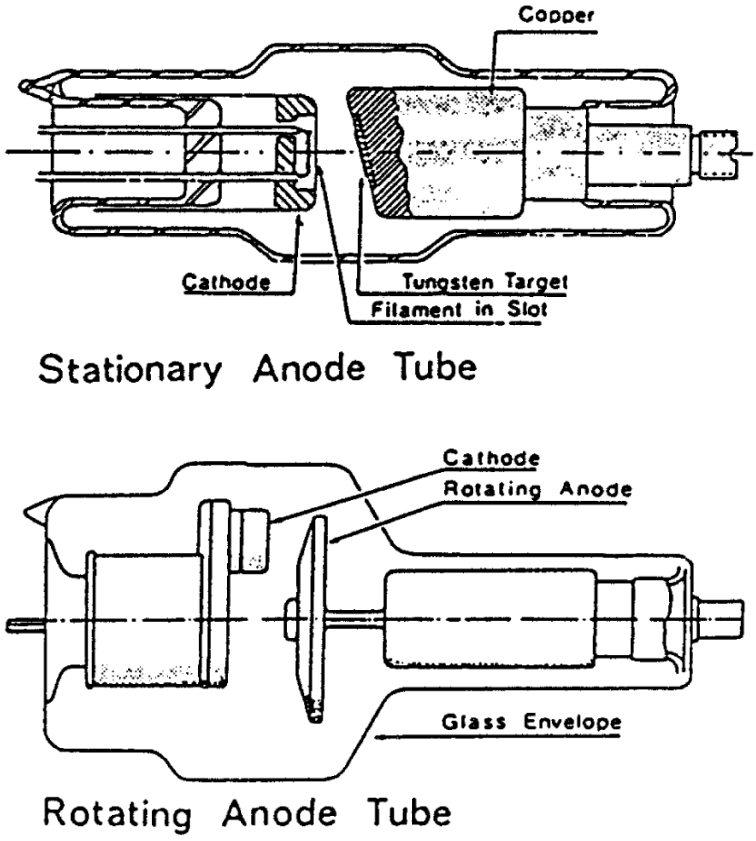

Figure 2.3: Schematic view of static (top) and rotating (bottom) anode tub.

For certain applications, in particular computed tomography (see later), the high voltage used in the tube for the acceleration of the electrons has to be extremely stable in order that the x-ray spectrum is constant in time. For the same reason, the stability of the electron beam hitting the target is an important aspect.

3. Absorption of x-rays

In the energy range which is used for diagnostic medical imaging (ca. 30–200 KeV) two absorption effects occur when the photons interact with material, *viz.*,

1. *photo effect* (*Fig. 3.1 a*)
2. *Compton effect* (*Fig. 3.1 b*)

The photo effect is a process where a photon is absorbed by an electron which is ejected from its shell to a higher energy level within the atom or completely removed from the atom (ionisation). The photon energy must at least correspond to the energy difference between the two electron states in question, i.e., to the difference between the initial and final state of the excitation process (multiphoton processes are not observed with the photon fluxes used in medical imaging). When the absorption spectrum of a material which consists only of one type of atoms is considered, “edges” are therefore observed which correspond to the energy levels associated with the various electron shells (K-, L-, M, etc.). As the

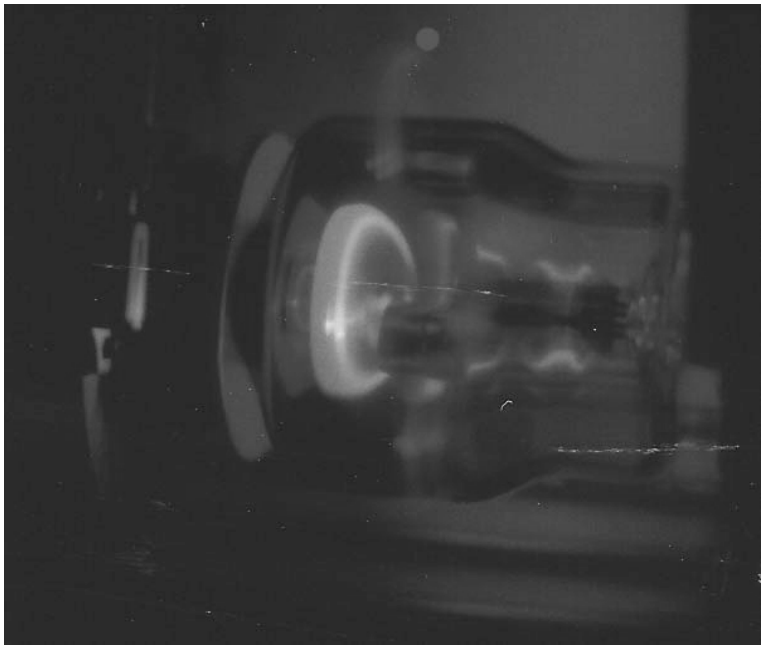

Figure 2.4: Red hot rotating anode under typical working conditions (courtesy: Comet AG, Bern).

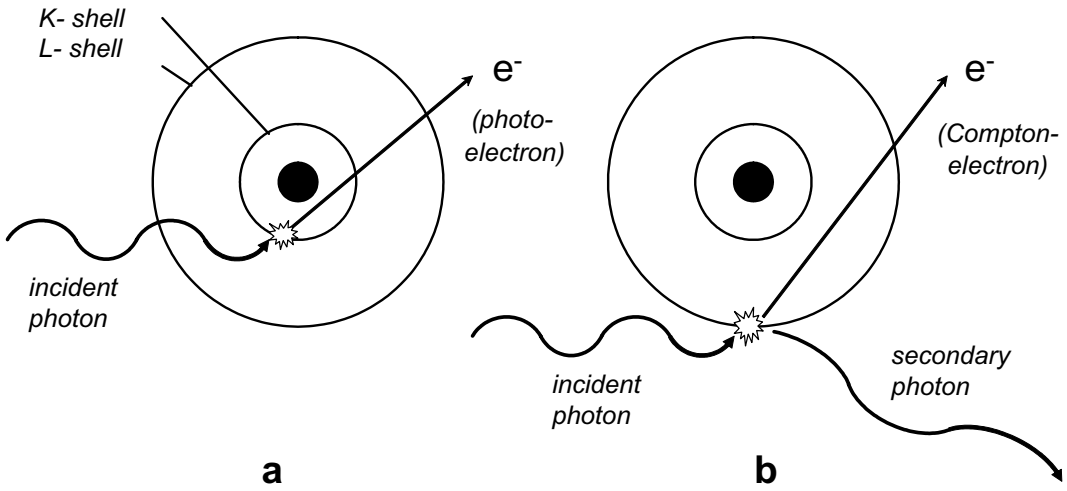

Figure 3.1: Photo effect (a), Compton effect (b).

K-electrons exhibit the highest binding energy, the K-edge is encountered first on the energy scale when approached from above (see Fig. 3.2 a). This property is being used in the energy subtraction method (see later).

With the Compton effect (Fig. 3.2 b), occurring at higher energies, a photon is likewise absorbed by an electron which is thereby excited, but there is excess energy which is emitted at the same time in the form of a lower energy secondary photon. These secondary photons represent scattered radiation since their direction does in general not coincide with the one of the original photon. They have a blurring effect and may lead to such a high noise level in an image that countermeasures have to be taken (collimators,

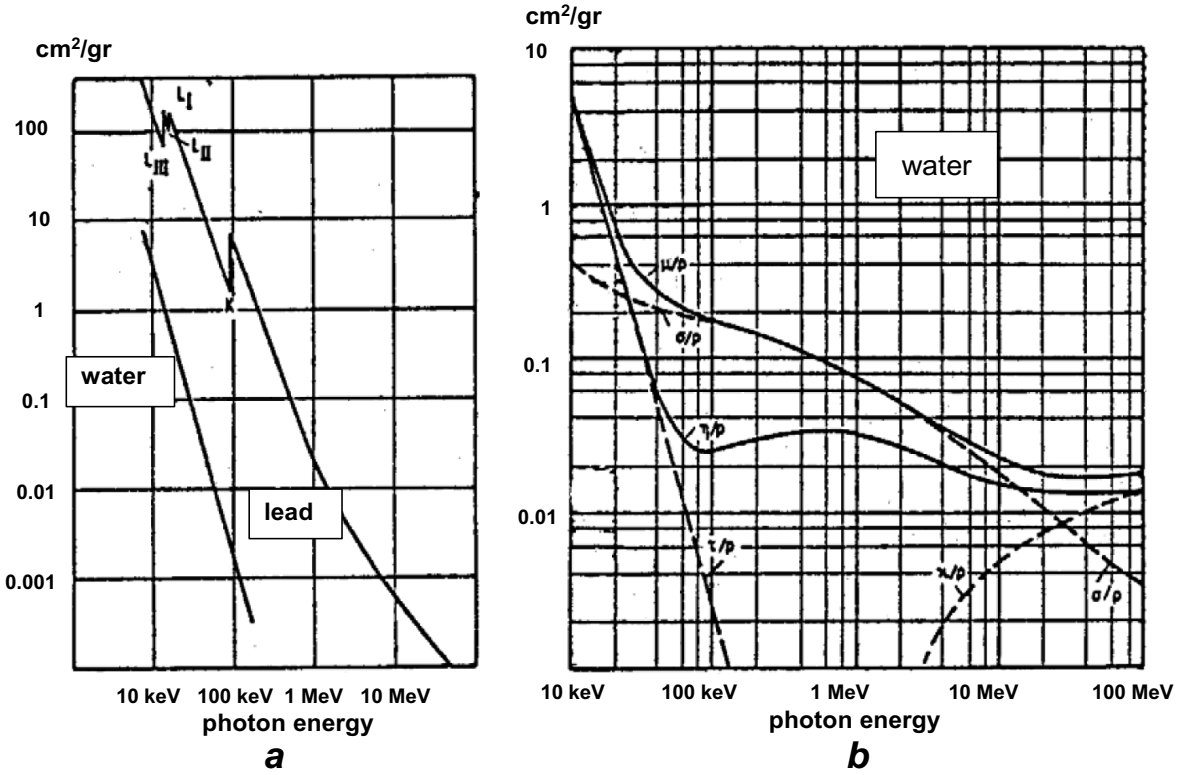

Figure 3.2: a: Mass absorption coefficient (photoeffect alone) for lead and water. b: Total mass absorption coefficient $\mu' = \mu/\rho$ (the definition of μ is given below, Beer-Lambert's law) as function of the photon energy, E. It is composed of the contribution of the photoeffect (τ/ρ), of the Comptoneffect (σ / ρ) as well as the one of pair production (κ / ρ). The latter effect is not considered here because for the production of an electron-positron pair an energy of at least 2 $m_0c^2 = 1.022$ MeV is necessary (m_0 = electron mass, $9.11 \cdot 10^{-31}$ kg). Since this energy is much higher than what is used in medical x-ray imaging, this effect is not of importance here (the additional curve, η/ρ, in the graph, is related to the energy conversion).

anti scatter grids, see below).

Since the Comptoneffect requires on the average a higher amount of photon energy, at lower energies the photoeffect prevails while at higher energies the Comptoneffect sets in.

The cross section of an atom with respect to a certain interaction process is defined as the (theoretical) area σ (in cm^2) perpendicular to the incoming radiation which – much like the target in a shooting range – is available for the initiation of the process in question. If the photon hits this area, the effect is triggered, if not, no interaction takes place. In order to obtain the specific absorption capacity (per unit of mass) of a material, the cross section has to be multiplied by the number of atoms per unit of mass. Accordingly, the mass absorption coefficient is defined as the total cross section per gram, i.e.,

$\mu' = \sigma \quad N_A/A$ (N_A Avogadro's number, A atomic weight)

Since N_A indicates the number of atoms per A grams of a substance ($6.023 \cdot 10^{23}$), the quotient N_A/A corresponds to the number of atoms per gram, i.e., μ' has the dimension cm^2/g.

With regard to medical imaging, the dependence of the mass absorption coefficient on the atomic number, Z (= number of protons in the nucleus), is decisive. Because of this dependence, the various biological tissues in the body exhibit different x-ray absorption characteristics such that their appearance in the projection image (grey level) varies according to their chemical composition. In case of the photo effect, σ is about proportional to Z^5, while for the Compton effect it is about proportional to Z. For

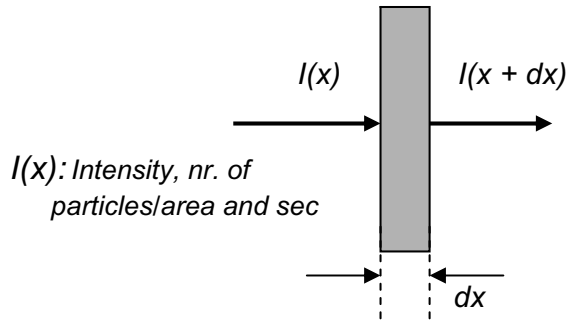

both effects, however, the cross section decreases with increasing energy, i.e., the penetrating power of the x-rays increases (Fig. 3.2). According to the object to be imaged, therefore, the voltage of the x-ray tube is set.

In total, the relation holds $\mu' = \mu/\rho = \tau/\rho + \sigma/\rho + \kappa/\rho$

Because of the stochastic nature of the occurrence of the various effects, the attenuation of an x-ray beam when penetrating a thin sheet (thickness *dx*) is proportional to *dx*,

$$I(x + dx) - I(x) = -\mu dx$$

which yields

$$I(x) = I_0 exp(-\mu x)$$

(Beer-Lambert's law). The linear attenuation coefficient, μ, is determined from the mass absorption coefficient introduced above according to $\mu = \mu' \rho$ ($\rho =$ density), because the entire mass of the material in the layer *dx* has to be taken into account. In case of composite materials or mixtures (as is always the case for biological tissues) the total mass attenuation coefficient μ'_{tot} can be determined from a weighted average (according to the density) from the individual coefficients of the various components.

As mentioned above, biological materials are always composed for various constituents in different concentration such that they can be distinguished according to their x-ray absorption properties (Fig. 3.3). These effects are systematic and reproducible.

4. X-ray projection imaging

4.1. Resolution of imaging procedures

From a technical point of view the resolution provided by an entire x-ray imaging chain (x-ray tube → image presentation) has to be considered. One has thereby to distinguish between

a) *spatial*
b) *contrast*
c) *temporal resolution.*

Only linear mappings are considered here.

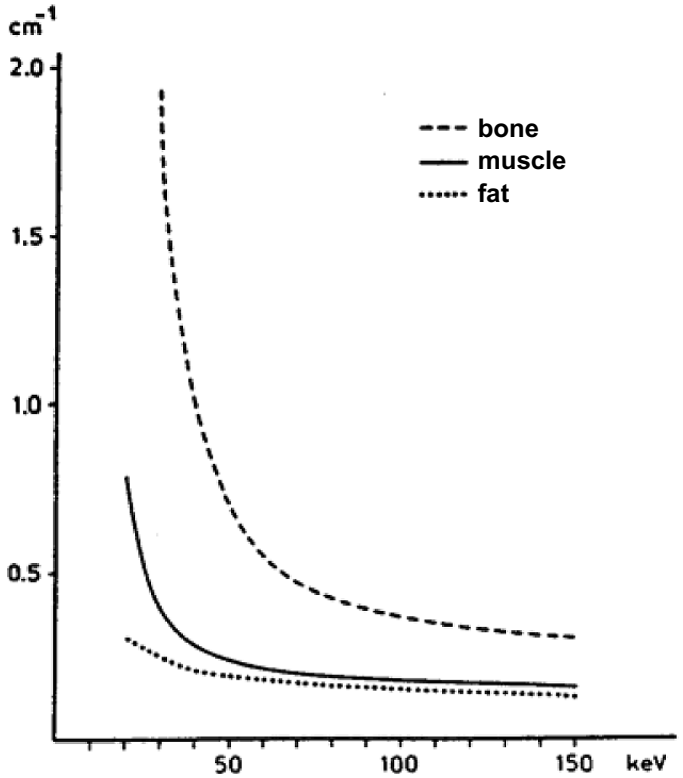

Figure 3.3: Dependence of the linear attenuation coefficient on the energy for various tissues.

4.1.1. Spatial resolution

The *spatial* resolution of an imaging chain is often given in terms of the normalized intensity amplitude as a function of line pairs / mm (lp/mm), denoted as Modular Transfer Function (MTF). The practical procedure to measure the MTF for x-ray systems consists of imaging lead grids of variable spacing (Fig. 4.1.1). The closer the lines are together, the smaller is the amplitude of the image and the average grey level increases until the lines cannot be discerned any more. The maximal amplitude (1) is defined as the maximal intensity step that can be represented. Typical MTF curves are shown in Fig. 4.1.2.

Instead of the MTF, the line spread or point spread function (LSF, or PSF), respectively, are sometimes given. These functions indicate onto what image a line or point is mapped.

In the Appendix 1, a mathematical derivation of the MTF is given. It can be shown that the MTF and LSF or PSF (in two dimensions) are related by a Fourier transform. Since every object (one or two dimensional) can be thought to be composed of lines (one-dimensional image) or points (two-dimensional image), in case of a linear mapping it is sufficient to know the LSF or PSF, respectively, to determine images. This procedure is often used in medical imaging.

Note: In the past, video techniques have often been used besides photographic film to visualize, record and store x-ray images, in particular when dynamic sequences such as imaging of the heart in the catheter laboratory were made. Conventional video images consist of distinct analog lines (*15'625 sec* $^{-1}$ *line frequency, 625 lines per full frame in case of the PAL norm*), *therefore, the MTF concept cannot be applied as such for TV-based images because of their inherent anisotropy. However, typical x-ray projection techniques yield images with considerably higher spatial resolution than corresponds to conventional TV, accordingly, high resolution digital image recording and presentation techniques are increasingly*

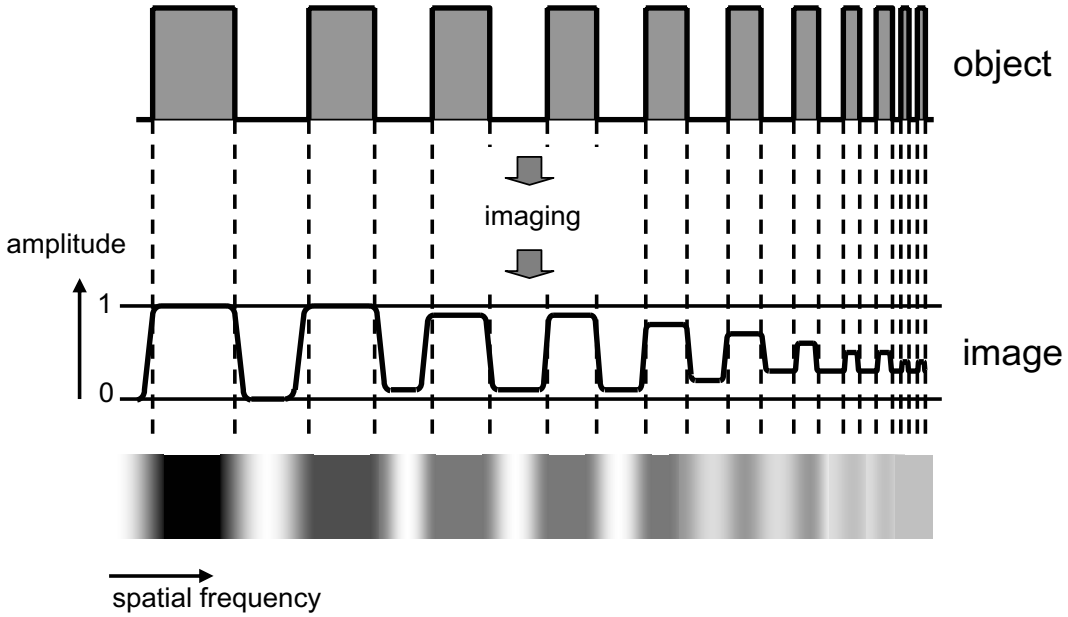

Figure 4.1.1: Imaging of a lead grid. With increasing spatial frequency (lp/mm) the amplitude of the image (grey level) decreases.

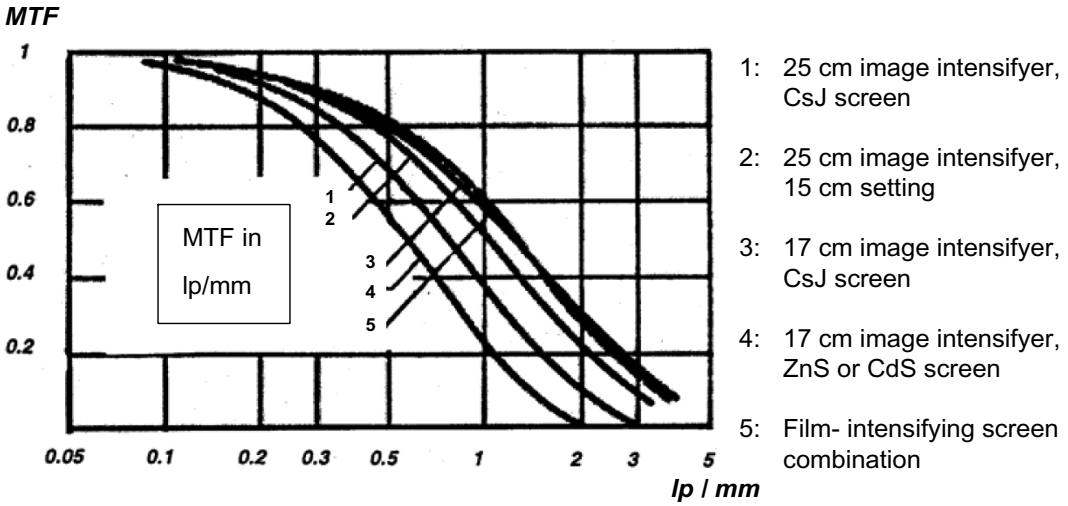

Figure 4.1.2: MTF of various x-ray systems (system definition see later).

being used and conventional TV gradually disappears for this purpose.

4.1.2. Contrast resolution

In order to assess the *contrast* resolution of x-ray projections, the contrast in the radiation behind an object has to be considered. As an example, we determine the intensity of an x-ray beam after passing through $d = 20$ *cm* of typical biological tissue:

$$I = I_0 \exp(-\mu d), \text{ or } I/I_0 = \exp(-\mu d)$$

Figure 4.1.3: Principle of the point spread function (PSF).

With $\mu = 0.35$ cm^{-1} (average for biological tissue devoid of bone and air) we obtain a contrast of exp (-7), i.e., about 1/1000. In the presence of bone and air (lung, intestine) the contrast is even considerably higher. Neither with photographic film nor with conventional TV such a contrast range can be recorded (film, as shown below, has a linear gray scale range of about 2.5–3, corresponding to a contrast range of about 1/300 to 1/1000, while conventional TV has less). Depending on whether, e.g., the lung, other soft tissues or bones are to be imaged, the radiologist has to choose the parameters anode voltage, anode current, exposure time in order to keep the desired contrast within the available range.

Digital imaging techniques allow to record images with an extended contrast range (12–16 bit resolution). Typical TV monitors, however, visualize only a limited grey level range of about 6 bit. Since images are stored in digital form, the visible contrast range can be selected and altered up and down in real time ("windowing").

4.1.3. Temporal resolution

The *temporal* resolution is of importance whenever dynamic processes are to be investigated (phlebogram, ventriculogram, stomach-intestine passage, *etc.*). Cassette changers (see later) reach a frequency of up to about 6 images/sec which is sufficient, e.g., for phlebograms. In order to resolve a heart cycle adequately, up to 50 images/sec are necessary (in the PAL norm, 50 half frames per sec are defined, 2:1 interlacing).

4.2. Photographic x-ray film

Diagnostic x-ray cause precipitation of silver bromide in a photographic emulsion such that x-ray intensity is reflected as grey level after development. A sharp image is only obtained, if the photographic layer is thin because of the mostly oblique incidence of x-rays in a projection arrangement. Besides, there is always undesired scattered radiation. Since the absorption in the photographic emulsion increases exponentially with the thickness (Beer-Lambert's law), in a typical x-ray film only about 2% of the incident radiation is absorbed. If not highest resolution is necessary (e.g., mammography or dental applications) double-sided film is used in order to increase the thickness (Fig. 4.2.1):

The low efficiency (requiring a correspondingly high radiation dose delivered to the patient) can be increased by adding intensifying screens on both sides of the film which is then called a cassette. This increases the absorption but decreases the resolution. The intensifying screen contains e.g. $CaWO_4$, a substance which exhibits blue fluorescence under the incidence of x-ray which increases film exposure (other fluorescent substances include Y_2O_2S, Gd_2O_2S, BaFCl). The efficiency can so be increased by a factor of about 5.

The opacity $1/T$ (inverse transmittance, dimensionless) of a (processed) photographic sheet is defined as

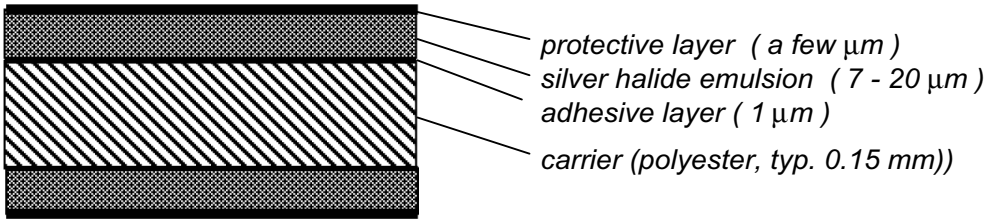

Figure 4.2.1: Composition of a typical photographic x-ray film.

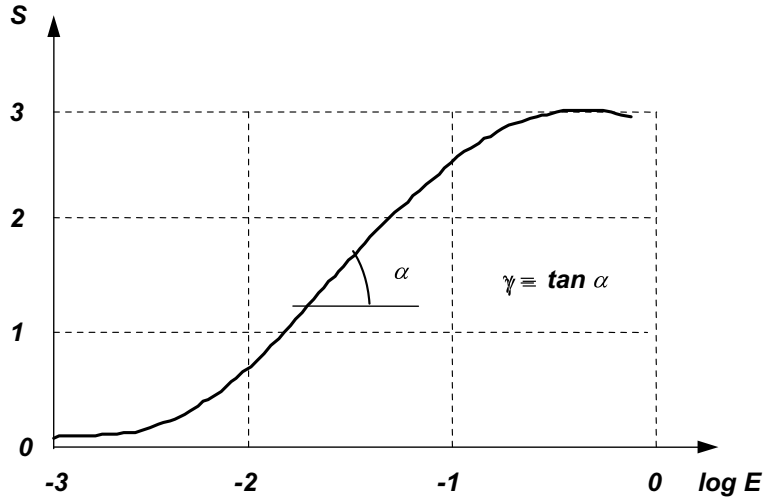

Figure 4.2.2: Typ. characteristic curve of photographic film [*S* : *log*(*opacity*), *E* : *exposure* (*in meter-candle-sec*)].

$1/T = (I_0/I)$ (I_0: incident, I: behind the sheet densitometrically measured intensity or brightness of a normalized

white light source, unit Lumen [Lm])

The density S[= *log*(*1/T*)] as a function of the exposure (characterizing the quantity of light delivered to the emulsion) of photographic film follows the diagram shown in Fig. 4.2.2.

The γ value of a film is a measure of the maximum change of film density for a certain change of exposure. This corresponds to the part of the characteristic curve with the steepest slope, i.e., at the point where the maximum derivative is found (= tangent of the inclination angle α). Typical photographic film has a linear range of about $\Delta\, S = 2.5$.

To eliminate scattered radiation, anti-scatter grids are used. Such grids are characterized by the distance and thickness of the lamellae (typ. 25–50 lamellae/cm) as well as the grid ratio (height of the lamellae/distance, typ. 5–15).

X-ray films are mostly used for single-shot static exposures. If slow processes are to be examined (e.g., in case of a phlebogram), cassette changers are applied which allow to take up to about 6 images/sec. The advantage of this procedure consists of the high image quality which corresponds to the one of x-ray film. If higher frame rates are required (e.g., for imaging of the heart), other procedures have to be applied, in particular in order to avoid excessive radiation doses (see later, image intensifier).

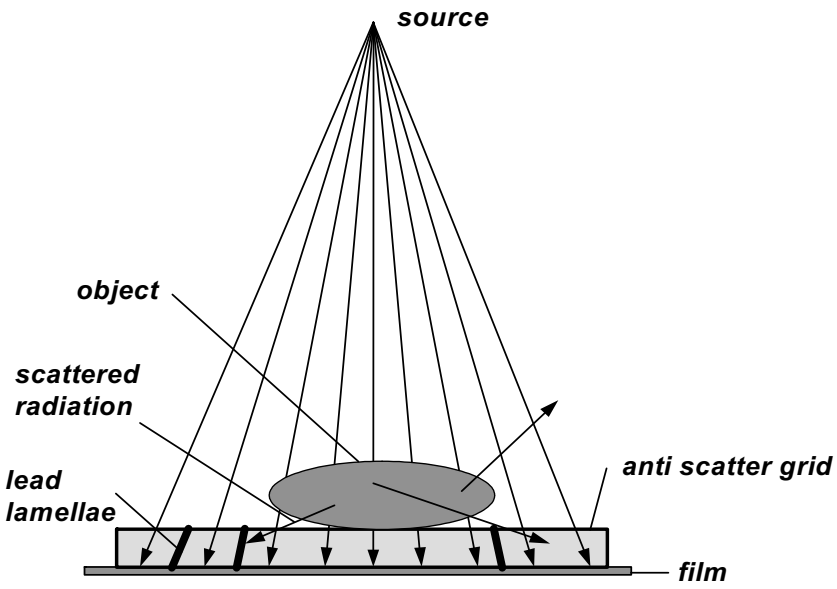

4.3. Direct digital x-ray → image conversion

Photographic film is an analog storage medium and preparation for computer analysis and archiving including networking necessitates off-line digitization. In addition, film development requires chemistry (cost and waste). A number of methods have therefore been developed which allow for a direct digital image acquisition.

Digital Luminiscence Radiography (DLR), Storage Screen Radiography, Computer Radiography (CR, Fig. 4.3.1)): On a screen made of BaFBr:Eu^{2+} (Europium-doted barium halegonide) a latent image is created by irradiation (excited electron states) which is converted off-line into visible fluorescence by laser scanning. One of the advantages of this technology consists of its large dynamic range.

Selenium-based detectors: Prior to the exposure to x-ray, the surface of the detector is charged electrically. The photons are converted into electrical signals in that they create charges in the interior of the selenium layer which neutralize the surface charges. Again, a latent image is formed which is scanned off-line.

Flat screen detectors on the basis of amorphous silicium: On a silicium wafer a pixel matrix containing the necessary electrical components (transistors) is implemented which allows for a direct digital conversion of the charges created by the incident x-rays Because the absorption of x-ray by silicium is only weak, additional layers containing heavy atoms have to be overlaid on the silicium screen.

Scintillator-fiberoptic-CCD chip arrangement (in the future also the much simpler and less expensive CMOS technology will be used instead of CCD): For particular applications, (e.g. μCT) a scintillator screen serves for spatially resolved photon acquisition which is imaged on a CCD chip by fiber optic connection. The possibility thereby exists for image enlargement by cutting the fiber optic bundle obliquely.

4.4. X-ray image intensifyer

In a x-ray image intensifyer (Fig 4.4.1) the radiation image is converted into an equivalent electron image in the entrance screen. The conversion occurs in two steps: First, light flashes are created in thin

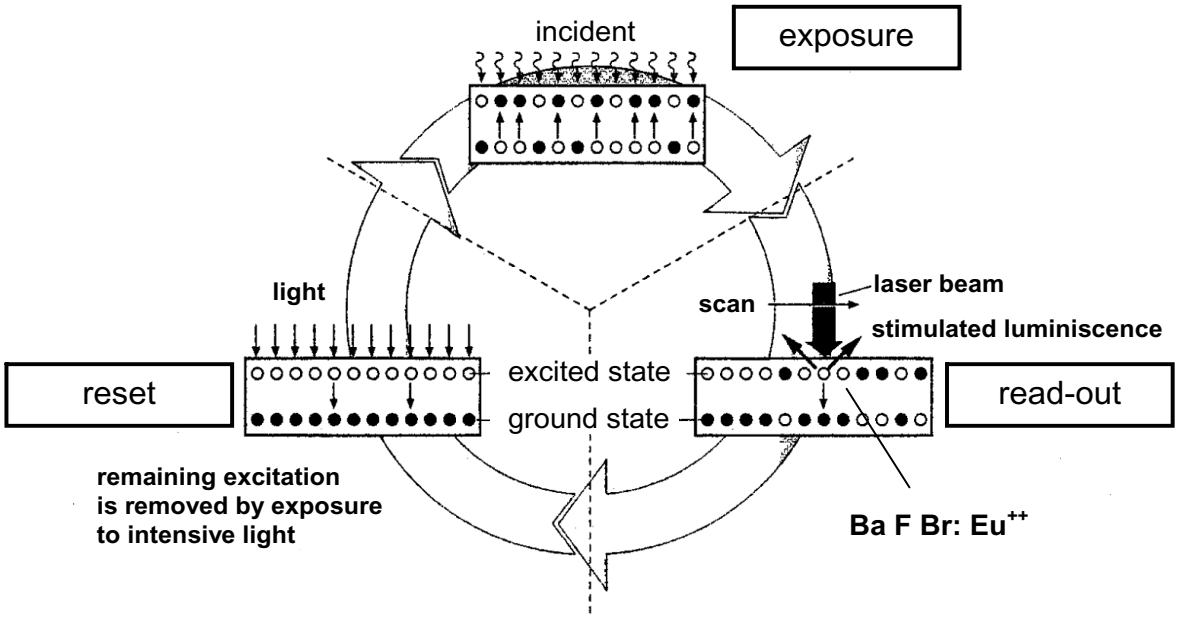

Figure 4.3.2: Principle of digital luminescence radiography.

CsJ needle crystals (scintillator) which are about 0.5–1 cm long (good absorption of x-ray) and densely arranged perpendicular to the screen in order to suppress scattered radiation as well as lateral diffusion of light (veiling glare). These light flashes cause the creation of free electrons in the photocathode which is connected to the scintillating screen. In addition, on the entrance side of the scintillator a thin aluminum foil is located which reflects light back onto the photocathode. The electrons whose lateral diffusion in the photocathode adds to the veiling glare and has therefore to be suppressed, are accelerated by 25 kV typically and directed towards the exit screen. Thereby, an electrostatic field acts as an imaging electron-"optics" such that a bright image on the exit screen appears. The intensifying effect is due to the kinetic energy which the electrons obtain during acceleration. The exit screen is recorded digitally, in the past, video or cinéfilm was used (up to 50 images per sec). Thanks to the good absorption properties of the entrance screen, the efficiency of present intensifiers is about 40–50%, i.e., substantially larger than film/intensifying screen combinations. The efficiency is given by the conversion factor G in $(\mathrm{cd/m^2})$ / (mR/sec) whereby cd (candela) denotes the light intensity $dI/d\Omega$ (light intensity or light flux per solid angle), mR (milli-Röntgen), the radiation dose (old unit).

5. Image subtraction techniques, Digital Subtraction Angiography (DSA)

The lumina of blood vessels, stomach, intestine, ventricles of the heart or of the brain are only faintly or not visible on a routine x-ray projection image. In order to obtain a diagnostically useful visualization, the lumen in question has to be filled with an appropriate contrast agent (e.g., bariumsulfate in case of stomach-intestine, or a compound containing iodine for blood vessels or the heart which is well tolerated, i.e. which causes no immune reactions).

To image a section of an arterial vessel (e.g., if an aneurysm, a stenosis or a dissection is suspected) or of a ventricle of the heart it is necessary to administer the contrast agent at the very location under consideration (selective catheterization) in order to obtain sufficient image contrast. This procedure is

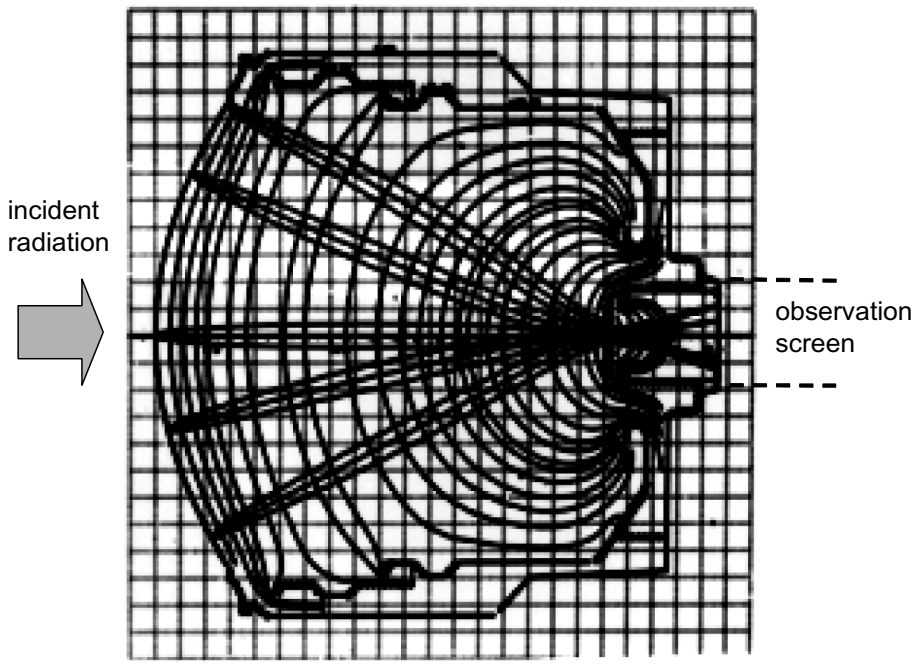

Figure 4.4.1: Cross section through image intensifyer showing electron paths and field lines.

associated with a considerable expense (catheter laboratory) since an arterial vessel has to be opened, furthermore, there is always the danger of an afterbleeding. In contrast, a venous infusion of a contrast agent is largely without problems. Although part of the contrast agent arrives at the location to be imaged on the arterial side also if a venous administration is made (e.g., through the vena cava), the resulting image contrast is insufficient because of the dilution of the contrast agent after the lung passage necessary to reach the arterial side and the subsequent distribution in the entire vasculature of the body. In addition, not only the location of interest contains therefore contrast agent, but all adjacent, overlying and underlying vessels including capillaries and veins such that the image of the vessel section in question is embedded and covered by other vessels.

With the aid of image subtraction techniques, however, an increase of contrast can be reached such that at least in the case of not too small arterial vessels a sufficiently good representation for diagnostic purposes can be obtained also with venous administration of contrast agent. Since for this technology on-line digital image treatment is applied, the method is called Digital Subtraction Angiography (DSA). (Note: Image subtraction can also be made easily with photographic film in that a negative can be obtained from contact exposure; for medical purposes, this procedure has been in use since about 1935). With DSA, an image called “mask” is first made (a digital projection image before the contrast agent is administered) and stored in the computer. Then, the contrast agent is applied transvenously, mostly through the vena cava. After about 20 sec, the exact time delay thereby depending on the location to be imaged, the contrast agent appears in diluted form at the desired section on the arterial side. Image sequences can now be acquired whereby the mask is subtracted in an on-line fashion (video, Fig. 5.1). Providing that the patient has not moved (among other, breathhold is necessary) between the acquisition of the mask and the later images, only the difference between the images, i.e., the shadow of the contrast agent should be visible.

Overlay is still present, but above all, noise amplification occurs since images characterized by small differences associated with noise are subtracted and subsequently amplified. Since minimal exposure

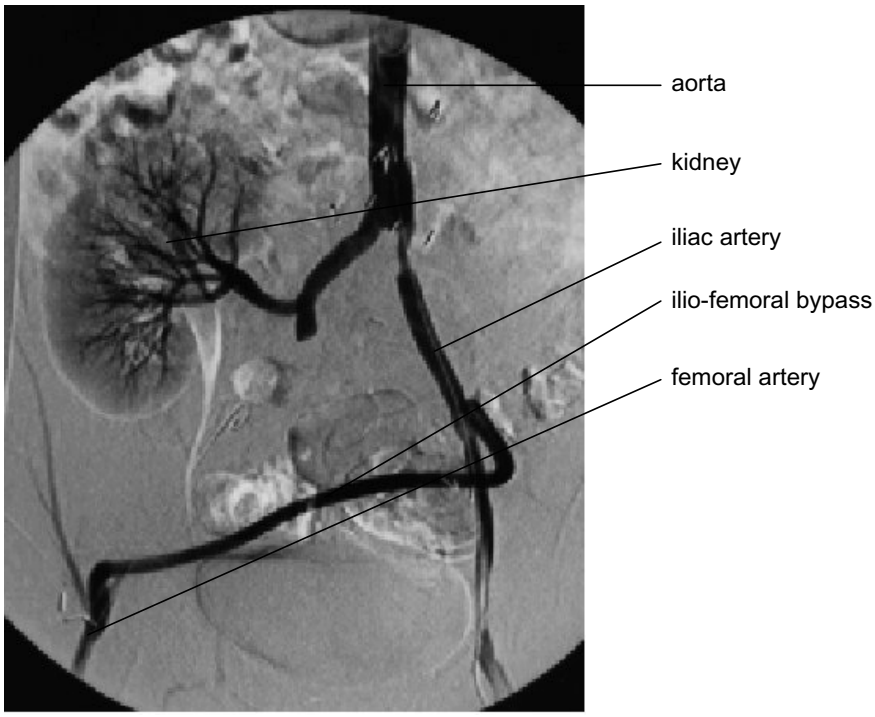

Figure 5.1: DSA image (real-time video subtraction) of a highly pathologic abdominal vessel situation.

to radiation is desired, the discrete nature of x-ray may become apparent ("quantum noise"). This can partially be compensated by using more contrast agent and/or a higher radiation dose, both of course undesired (on the one hand, the incidence of immune reactions increases with an increasing amount of contrast agent, on the other, a higher radiation dose is undesired anyway). In spite of these drawbacks, the advantage of avoiding an arterial catheterization is by far dominating such that DSA is applied whenever possible.

6. Computed tomography (CT)

Computed tomography[1] (derived from greek $\tau o \mu \varepsilon \iota \nu$, to cut) was introduced in 1973 by G.N. Hounsfield in England (Fig. 1.2). A.M. Cormack in South Africa had in fact already earlier investigated methods which allowed to reconstruct objects from a series of suitably chosen x-ray projections (Hounsfield made his later work however independently from Cormack's results). Since at the time when Cormack made his investigations there were no reasonably priced computer-assisted imaging methods available, he could not represent the results of his calculations as true tomograms, i.e., images of cross sections, but just in the form of numbers and curves, accordingly, his work had no practical consequences (nevertheless, both researchers received the Nobel prize in 1979). What both researchers did not know,

[1]The "classical" tomographic procedure in radiology was performed in such a way that the x-ray source (tube) and the photographic film were shifted during the exposure continuously in opposite directions. Only one plane is thereby imaged sharply, structures which are located underneath or above this plane are smeared. The images have therefore a low contrast, however.

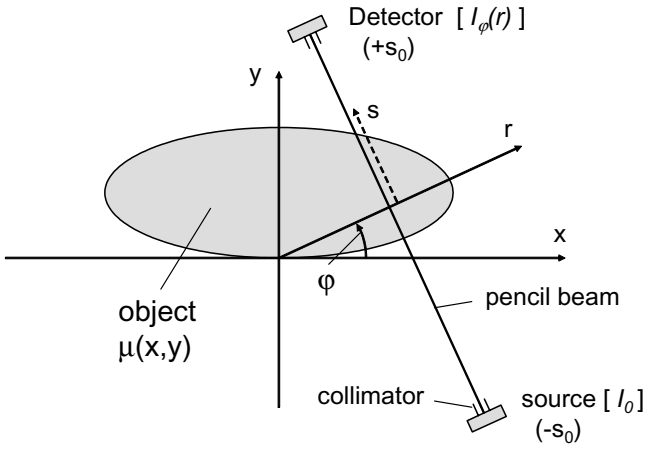

however, was the fact that the mathematical problem of calculating a n-dimensional object from $n-1$ dimensional projections had been solved much earlier by the Austrian mathematician Johann Radon (1887–1956) already in 1917. This was recognized only after CT had been introduced into clinical routine. Yet, this was not of importance because Radon's formal mathematical solution was found to be unsuitable for practical applications for numerical reasons.

The method of CT consists of the acquisition of a sequence of x-ray projections of a predetermined cross section of the body under different angles. In scanners of the first generation, a single projection was taken by translating a collimated x-ray beam ("pencil beam") over the chosen cross section. This procedure required a synchronous movement of the source (x-ray tube) and the detector. Later, the "fan" beam technology was introduced whereby an entire projection is taken at the same time with the aid of a detector array. (consisting, e.g., of 512 detectors) without translation of the x-ray source. Subsequent rotation of the x-ray source and detector array around 180° in equally spaced angle intervals (e.g., 180°/512) further projections are taken (Fig. 6.1). A total set of (one dimensional) projections then allows to reconstruct the interior of the cross section, i.e., the two-dimensional distribution of the attenuation coefficients $\mu(x,y)$ (x,y are Cartesian coordinates in the cross section) The image is represented in the form of a grey level distribution $D(x,y)$. In present scanners, the fan beam – detector array is rotated and advanced in a spiraling motion around the patient such that entire spatial body sections can be imaged within a few seconds (Fig. 6.2).

For simplicity, we consider the situation of a first-generation translation-rotation scanner. The beam intensity, $I_\varphi(r)$, which is recorded in a direction perpendicular to a fixed angle φ as function of the linear coordinate, r, is obtained as

$$I_\varphi(r) = I_0 exp\left\{-\int\limits_{-s_0}^{s_0} \mu(s[r,\varphi])ds\right\}$$

where I_0 denotes the intensity of the unattenuated beam (before impinging on the object) and $s[r,\varphi]$ is the line defined by $r$and φ between source and detector in the $x-y$ plane. The integration is performed along the line s from $-s_0$ to$+s_0$ (distance between source and detector).

As projection $P_\varphi(r)$ the quantity

$$P_\varphi(r) = \log[I_\varphi(r)/I_0] = -\int\limits_{-s_0}^{s_0} \mu(s[r,\varphi])ds$$

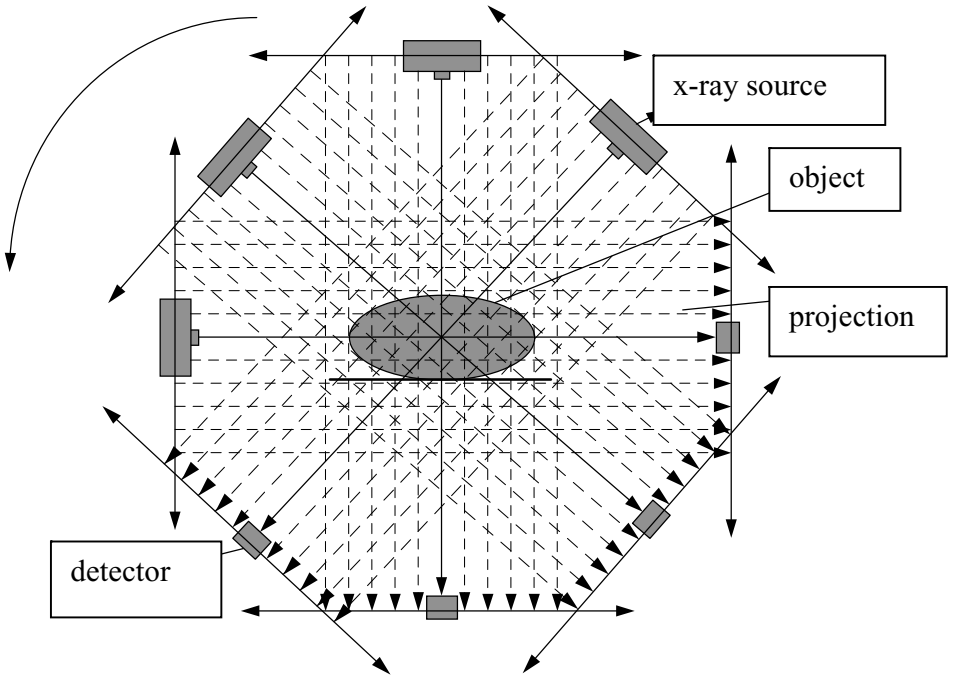

Figure 6.1: Principle of first generation CT scanner: A narrow x-ray beam (pencil beam) is generated by collimators at the x-ray source as well as at the detector (the latter primarily suppresses scattered radiation). One-dimensional projections are obtained by translating the unit (embedded in a gantry) over the object. By successive rotation of the gantry after each translation by, e.g., $\pi/512$, a complete set of projections is recorded.

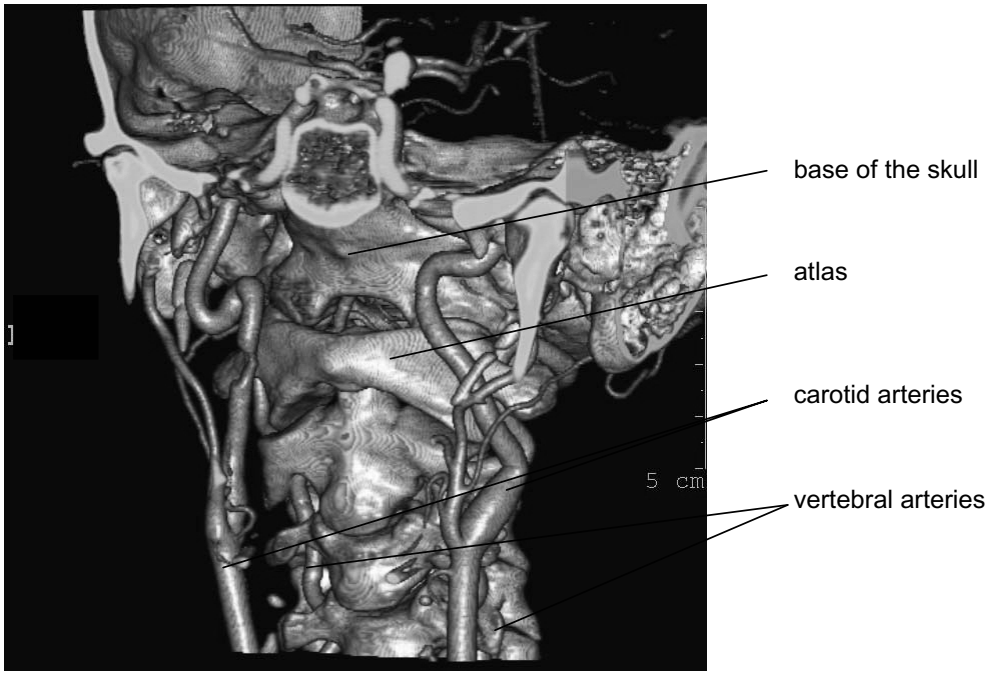

Figure 6.2: Spiral CT image of the base of the skull (after segmentation).

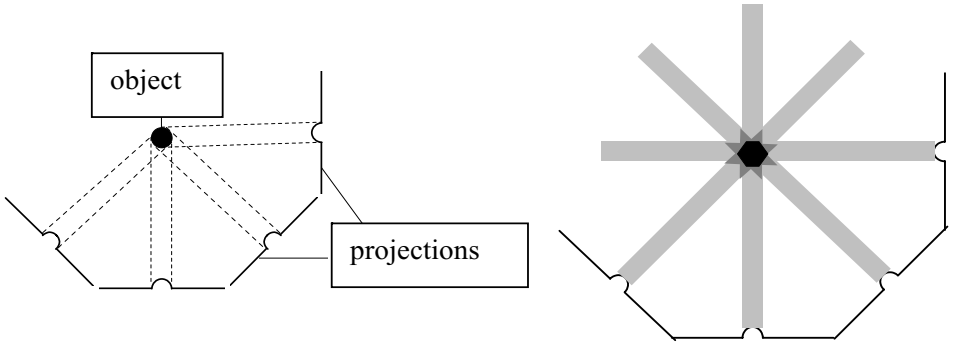

Figure 2.5.2: Schematic representation of four projections (left) of a cylindrical, homogeneous object and corresponding simple backprojection (right). The measured projection values are thereby distributed homogeneously ("backprojected") over the projection path. The resulting "reconstruction" is characterized by star-like artifacts, moreover, the image of the cylindrical cross section extends over the entire scanned area. If the radius of the cylinder is assumed to approach zero and the number of projections is increased to infinite, the point spread function (PSF) is theoretically obtained.

is defined. The task now consists of the determination of the linear attenuation coefficients, $\mu(x, y)$, from a complete set of projections $P_\varphi(r)$.

As mentioned above, Radon found an analytic solution of the problem, which is unsuited for a numerical application, however. Among the various methods which have been evaluated for the calculation of the grey scale image $D(x, y)$ derived from the attenuation coefficients $\mu(x, y)$, the method outlined in the following called convolution / backprojection has proven to be particularly useful.

A simple backprojection without further pre- and postprocessing of the data is performed by distributing the entire value of the integral $P_\varphi(r)$uniformly along the projection path, s (Fig. 6.3). As an example, we consider the projection of a cylindrical object which is scanned perpendicularly to its long axis. If it is assumed that (i) the radius of the object $\rightarrow 0$, (*ii*) the number of projections (angles) $\rightarrow \infty$, and (*iii*) each one-dimensional projection is continuous, i.e., it consists of infinitely many points, theoretically, the image of a point results (point spread function, PSF). The PSF is found to be proportional to $1/r$, since along the perimeter of every concentric circle around the point under consideration the same amount of backprojection is accumulated.

According to Chapter 3.1. it suffices to know the PSF associated with the imaging procedure in order to be able to determine the image (i.e., the reconstruction) of any two dimensional object. The reconstruction problem would therefore be solved, if the "corrected" PSF was known, more precisely, if the mathematical procedure to be applied in order that a point appears as a point without artifacts was known. Accordingly, the artifacts present in the simple backprojection procedure, in particular the $1/r$ dependence, have to be compensated.

This is achieved by applying a prefilter (mathematical convolution) to the projections. It can be shown (Appendix 2) that a convolution of the form

$$P'_\varphi(r) = [1/(2\pi)^2] \int_{\infty}^{\infty} P^*_\varphi(u) exp[iur]|u|du$$

yields the desired result. The function $|u|$ thereby compensates the $1/r$ dependence as well as the fact that the Fourier space associated with the scanned area is not uniformly sampled (Appendix 2, this follows from the Fourier-slice theorem): High spatial frequencies are sampled less densely than low frequencies.

Appendix 1: The Modular Transfer Function (MTF)

The spatial resolution of imaging systems is often given in the form of the Modular Transfer Function (MTF, i.e., grey-level contrast in the image space as function of the number of line pairs/mm in the object space; we assume for simplicity the one dimensional case, object space coordinate x). This concept can be introduced as follows: Each (one dimensional) object, characterized by a grey-level or intensity function $O(x)$ can be thought to be composed of lines

$$O(x) = \int_{-\infty}^{\infty} O(X)\delta \text{ (x - X) dX}$$

by making use of the Dirac function $\delta(x - X)$. We assume now that the Line Spread Function (LSF), $L(x')$, which denotes the mapping of a line at location $x = 0$ in the object space, $i.e.$, of $\delta(x)$, onto the image space with coordinate x', is known. A line at location X in the object space with intensity $O(x)$ will then yield an image

$$O(X)\delta \text{ (x – X)} \rightarrow O(X)\ L(x' - X)$$

In case of an optical imaging system with lenses, e.g., the LSF will be a diffraction pattern, for x-ray projection images, the line will be blurred.[2]

A general object, $O(x)$, can be decomposed into Fourier components (providing that it fulfils the usual mathematical conditions) according to

$$O(x) = \int_{-\infty}^{\infty} [a(k)\sin(kx) + b(k)\cos(kx)]dk$$

with $a(k)$, $b(k)$ amplitudes
$k = 2\pi / \lambda$ wave number, wavelength λ
One component

$$J_k(x) = a(k)\sin(kx) = a(k)\int_{-\infty}^{\infty} \delta(x - -X)\sin(kX)dX$$

is imaged by way of the LSF into the image space as $J_k'(x')$in the form

$$J_k'(x') = a(k)\int_{-\infty}^{\infty} L(x' - X)\sin(kX)dX$$

Upon performing the transformation $x'' = x' - X$ and making use of the addition formulas for circular function, one arrives at

$$\begin{aligned} J_k'(x') &= a(k)[\sin(kx')\int_{-\infty}^{\infty} L(x'')\cos(kx'')dx'' - \cos(kx')\int_{-\infty}^{\infty} L(x'')\sin(kx'')dx''] \\ &= a(k)[\sin(kx')a_1 - \cos(kx')a_2] \end{aligned}$$

[2]For two dimensional images, the Point Spread Function (PSF) is used instead of the line spread function, in that a two-dimensional image can be decomposed into points, using the Dirac function in both dimensions.

With

$$\eta(k) = \{[\int_{-\infty}^{\infty} \cos(kx'')L(x'')dx'']^2 + [\int_{-\infty}^{\infty} \sin(kx'')L(x'')dx'']^2\}^{1/2}$$

and using the addition property of circular functions once more, the result can be written as

$$J_k{}'(x') = a(k)\eta(k)\sin(kx'-\varphi)$$

The Fourier component $J_k(x) = a(k)\sin(kx)$ is therefore imaged onto the image space as harmonic function of the same frequency, k, but displaced by the (spatial) phase φ and with the amplitude $a(k)\eta(k)$. The relation holds for every k.

The function $\eta(k)$is denoted as Modular Transfer Function (MTF), and it is seen that the relation holds $0 \leqslant \text{MTF} \leqslant 1$. This function describes the dependence of the amplitude of the original intensity function in the image space (which is always reduced) as function of the spatial frequency k. Since the relation holds for every k, one can conclude that

$$F(image) = MTF{\cdot}F(\text{original})(F : \text{Fourier transformation})$$

respectively, that the image corresponds to the convolution of the original with the MTF according to the convolution theorem.

The relation with the LSF (for two-dimensional images with the PSF) is seen from the definition of the MTF.

Appendix 2: The convolution/backprojection method

It was seen in Chapter 6, that a simple backprojection leads to characteristic artifacts, in particular, if the projections of a point object are backprojected, a 1/r dependence results. By prefiltering the projections, the artifacts can be compensated (or at least substantially reduced). This aim is best reached in an indirect way, since on the one hand the function $1/r$ exhibits a singularity and on the other it has to be noted that that the real scanning procedure (translation – rotation) is made in finite steps which – as will be seen below – leads to an inhomogeneous sampling in the Fourier space, or, in the real space, there are significant deviations from the theoretical $1/r$ – dependence.

First, the projection $P_\varphi(r)$ is Fourier transformed

$$F\{P_\varphi(r)\} = P^*_\varphi(u) = \int_{-\infty}^{\infty} P_\varphi(r)exp(-iur)dr = -\int \int_{-\infty}^{\infty} \mu(s[r,\varphi])exp(-iur)drds$$

(As mentioned above, the integration over $s$is extended to infinite for formal reasons, as outside the source – detector area we can assume $\mu = 0$.) Upon transformation of the variables $r = x\cos\varphi + y\sin\varphi$, $s = -x\sin\varphi + y\cos\varphi$ one obtains (the limits $\pm\infty$ are omitted)

$$\begin{aligned} -P^*_\varphi(u) &= \int\int \mu(s[r,\varphi])exp(-iur)drds \\ &= \int\int \mu(x,y)exp(-iu[x\cos\varphi + y\sin\varphi])dxdy \\ &= \int\int \mu(x,y)exp(-ix[u\cos\varphi])exp(-iy[u\sin\varphi])dxdy \\ &= \int\int \mu(x,y)exp(-ixp)exp(-iyq)dxdy|_{p=u\cos\varphi, q=u\sin\varphi} \end{aligned} \tag{1}$$

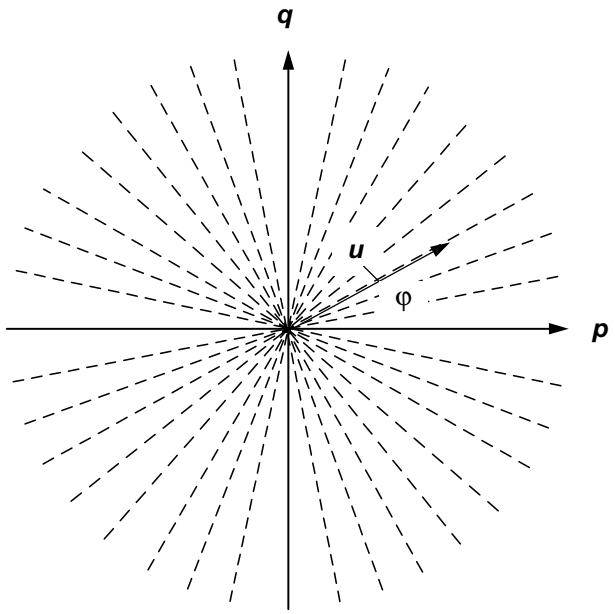

This implies that the Fourier transform of the projection $P_\varphi(r)$ corresponds to the two-dimensio-nal Fourier transform of $\mu(x,y)$ on a straight line which runs (in the two-dimensional Fourier space p,q) under the angle φ through the origin (Fourier – slice – theorem). The Fourier space is therefore sampled inhomogeneously in a star-like fashion in case of translation-rotation scanning. In particular, the high frequencies (image sharpness!) are covered less densely than the low frequencies. In order to recover the Fourier transform $P^*(p,q)$ of $\mu(x,y)$ with uniform density in the entire Fourier space of interest from the Fourier-transformed projections $P^*_\varphi(u)$, interpolations are necessary.

From the relation Eq. (1) can be seen that the reconstruction problem, i.e., the calculation of $\mu(x,y)$ can be solved by a reverse Fourier-transformation (after having determined the Fourier-transformed projections and interpolated $P^*(p,q)$). A two dimensional reverse Fouriertransform has however to be executed numerically for this purpose which is an unsuitable procedure. This can be prevented in the following fashion.

From the formula for the reverse Fourier-transformation

$$-\mu(x,y) = [1/(2\pi)^2] \int\int P^*(p,q)\ exp\ (ixp)\ exp\ (iyq)\ dp\ dq$$

one obtains after having transformed the variables according to

$$p = u\cos\varphi, q = u\sin\varphi, dp\ dq = u\ du\ d\varphi$$

$$-\mu(x,y) = [1/(2\pi)^2] \int_0^{2\pi}\int_0^{\infty} P^*(u,\varphi) exp[iu(x\cos\varphi + y\sin\varphi)]\ u\ du\ d\varphi$$

Upon making use of the symmetry of $P^*(u,\varphi)$($P^*[u,\varphi + 180^\circ] = P^*[-u,\varphi]$, since the same projection is recorded after a rotation of 180°) this expression can be written as

$$-\mu(x,y) = [1/(2\pi)^2] \int_0^{\pi}\int_{\infty}^{\infty} P^*_\varphi(u)\ \exp[iur]\ |u|\ du\ d\varphi$$

with $x \cos \varphi + y \sin \varphi = r$. By writing

$$P'_{\varphi}(r) = [1/(2\pi)^2] \int_{-\infty}^{\infty} P^*_{\varphi}(u) exp[iur]|u|du \tag{2}$$

and

$$-\mu(x,y) = \int \pi_0 P'_{\varphi}(r)d\varphi = \int_0^{\pi} P'_{\varphi}(x\cos\varphi + y\sin\varphi)d\varphi \tag{3}$$

one finds that this corresponds to a filtering or a weighting of the Fourier-transformed projections $P^*_{\varphi}(u)$with $|u|$ Eq. (2) before execution of the reverse transform, which now is restricted to one dimension. The subsequent integration over the angle φ is a summation over all weighted reverse-transformed projections and is equivalent to a backprojection Eq. (3).

On the basis of Eqs (2) and (3) the question relating to the PSF can finally be answered. According to Chapter 3.1. the convolution theorem reads ("*" denotes a convolution)

Image = PSF * Object, resp. F {Image} = F {PSF} $\cdot$ F{Object}

Here, "Image" denotes the reconstruction which is provided by the PSF and "Object" the true distribution of the linear absorption coefficients $\mu(x,y)$. The (two-dimensional) Fourier-transform of $\mu(x,y)$ is known, if measurements are made under all angles and the entire two-dimensional Fourier-space (p,q) is interpolated (it is however inhomogeneously covered by the one-dimensional Fourier-transforms $P^*_{\varphi}(u)$). Eq. (2) indicates that the factor $|u|$ compensates the artifacts. The inverse transform of $|u|$ would therefore correspond to the corrected PSF. Upon performing an inverse transform of the function $|u|$ exp (-$\varepsilon|u|$) for $\varepsilon \to 0$ ($|u|$ itself cannot be transformed!), a dependence $\sim 1/r^2$ is found. This can be interpreted such that the $1/r$ – dependence of the PSF (in simple backprojection) is additionally compensated by a further $1/r$ factor which is due to the inhomogeneous coverage of the Fourier space which also is characterized by a $1/r$ dependence.

If therefore for the backprojection (3) not the original projections $P_{\varphi}(r)$, but the corrected "projections" $P'_{\varphi}(r)$ are used, the desired results are obtained. In the object space, the procedure involves a convolution such that the method is denoted as convolution-backprojection method. It is the method of choice in computed tomography technology. If further effects which cause image deterioration are taken into account by adaptation of the kernel function $|u|$ still further improvements can be achieved.